

# The Hydrogen 21-cm Line and Its Applications to Radio Astrophysics

Lulu Liu (Partner: Chris Chronopoulos)\*

*MIT Undergraduate*

(Dated: March 9, 2008)

We explore some applications of the 21-cm neutral hydrogen line in astrophysics. From observations in a narrow band around 21 cm we find estimates for the peak temperature of the chromosphere of the sun, as well as the angular extent of a portion of the galactic plane around  $l = 30^\circ$ . We determine the rotation curve of the Milky Way galaxy (for  $r < R_\odot$ ) and explore its spiral structure for galactic longitudes  $30^\circ < l < 80^\circ$ . We find that the speed of rotation of the galaxy  $v(r)$  rises linearly in  $r$  from  $r = 0$  to  $r \approx 2.5kpc$  at which point it remains a constant up to at least  $R_\odot$ . This behavior deviates significantly from Keplerian predictions for large  $r$  and the expected rotational curve generated by all visible matter in the galaxy. It is clear that the current models for the dynamics of the Milky Way galaxy are insufficient to describe the actual physics of this system. A possible explanation lies in an extensive dark matter halo.

## 1. INTRODUCTION

It is well known in optics that as the wavelength of light increases, attenuation through a given material decreases. It is no wonder, then, that radio waves reach us from parts of deep space that optical light does not. In particular, clouds of interstellar gas that would otherwise hide optical features in our galaxy can reveal much about general galactic structure and dynamics if we look in a frequency band around 1420.4 MHz. This is known as the 21 cm line. Emitted by neutral hydrogen atoms, this line can be seen with varying intensity coming from all directions in the sky, and due to its extremely sharp nature (very little dispersion in energy), is used widely in astronomy for spectroscopic velocity measurements.

## 2. THEORY OF THE 21-CM LINE

A neutral hydrogen (H1) atom has one proton and one electron. Both particles have quantized total spin ( $s$ ) of  $1/2$  and a spin in the z-direction ( $m$ ) of either  $1/2$  or  $-1/2$ . Spin-spin coupling is the result. It was discovered that what was once thought to be a degeneracy in the ground state of the hydrogen atom is in fact a very fine energy level split between a more energetic parallel spin state  $|m_e = \frac{1}{2}, m_p = \frac{1}{2}\rangle$  and a less energetic anti-parallel ground state  $|m_e = \frac{1}{2}, m_p = -\frac{1}{2}\rangle$ . The perturbing Hamiltonian here is given by  $H' = -\vec{\mu}_p \cdot \vec{B}_e$ . When a hydrogen atom transitions from the excited state into the ground state, a photon is emitted carrying away the energy difference. This photon has a wavelength of 21 cm.

The spin-flip transition, as it is termed, is a highly forbidden process, with a mean-life of approximately  $10^7$  years. The Heisenberg Uncertainty relationship then leads us to expect a very sharp emission line with small  $\Delta E$  energy dispersion, or line width, in frequency. This

feature allows for highly accurate determinations of H1 source velocity by simple measurements of the doppler shift of the 21 cm line. Using the relativistic doppler shift formula, with  $\beta = v_{rec}/c$ ,

$$\nu_{obs} = \nu_{source} \sqrt{\frac{1 - \beta}{1 + \beta}} \quad (1)$$

we can obtain the recessional velocity,  $v_{rec}$ , by solving the equation for  $\beta$ .

## 3. EQUIPMENT AND TEMPERATURE CALIBRATION

For our experiment we have access to the Small Radio Telescope on the roof of Building 26 developed by Haystack Laboratories. A motor and feedback loop controls the pointing of the telescope. Radio signals received are fourier transformed and sorted into frequency bins in a multi-channel accumulated spectrum of counts converted to power (in K) against frequency.

A temperature calibration is performed internally by the electronics of the system. A noise diode emitting black body radiation at 115 K is activated at the vertex of the parabolic dish. The effect is a signal that fills up the entire antenna and is read by the feed horn. Subsequent signals are compared against this calibration and converted into an effective temperature reading that is proportional to the power received. The dish has a half-power beamwidth of approximately  $7.5^\circ$  [5]. We point our receiver to a patch of the cold sky (elevation  $> 50^\circ$ ) in order to perform our calibration and obtain a baseline system noise temperature,  $T_{sys}$ .

## 4. TELESCOPE POINTING (25-POINT SCAN)

We use the sun as a means of correcting pointing errors on the telescope. An "Npoint" scan of the sun creates a  $5 \times 5$  grid around a central point and takes a temperature measurement at each point in the grid. 25 temperatures

---

\*Electronic address: [lululu@mit.edu](mailto:lululu@mit.edu)

are recorded in all and can be used to create a temperature contour plot of the sun, see Figure 1. The telescope re-centers on the point of maximal temperature; the offsets are recorded. By using this method, we find a general repeatable pointing error of approximately  $2^\circ$ .

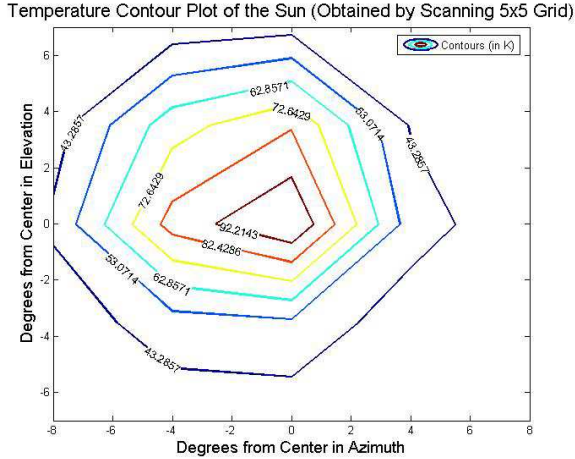


FIG. 1: A 25-point scan of the sky surrounding the sun. Contour curves are shown.

## 5. BEAM WIDTH DETERMINATION AND PEAK TEMPERATURE OF THE SUN

We point the telescope approximately 45 minutes ahead of the sun. By turning off the tracking mechanism, we allow the sun to drift through our antenna beam, taking integrated readings approximately 10 seconds apart. We then sum over the power recorded in each bin in order to obtain an average power per bin as a function of time. This manipulation, as well as the integration time, is factored into the error on each data point. Our results from the scan is given in Figure 2.

The Fraunhofer Diffraction pattern, intensity as a function of angle  $\theta$ , is described in the following relation involving the Bessel function  $J_1$  [4]:

$$I(\theta) = I_0 \left( \frac{2J_1(k \sin \theta)}{k \sin \theta} \right)^2 \quad (2)$$

The theoretical first minimum occurs at  $\sin \theta \approx \theta = 1.22\lambda/D$ . Here,  $\lambda = 21 \text{ cm}$  and  $D = 8.2 \text{ ft}$ . We find it to be  $5.87^\circ$  for our setup. Comparing with the  $2\sigma$  obtained from our gaussian fit, we find reasonable agreement, considering  $2\sigma$  is a slight underestimate of the first minimum of a corresponding Bessel function.

From the gaussian fit, we find a peak temperature of  $77.5\text{K}$ , which is far below any reasonable limit for the temperature of the sun. Corrections are applied to account for both the fraction of the beam width occupied by the sun (with an angular extent of approximately  $0.5^\circ$ )

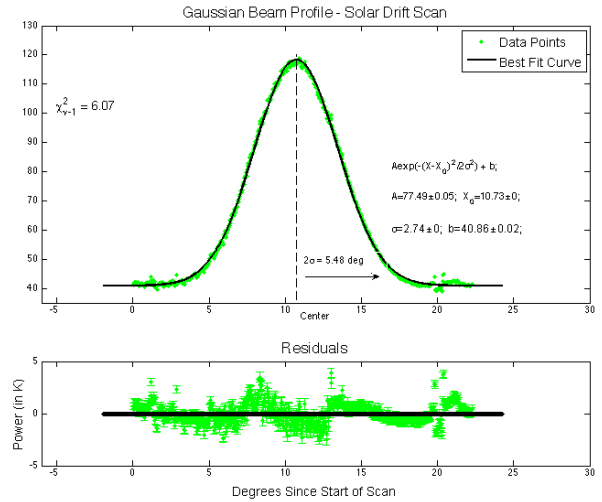


FIG. 2: Drift scan over the sun. The Bessel diffraction pattern is smeared out by the finite angular extent of the sun and the resulting curve is a reasonable gaussian fit. We use  $2\sigma$  on the gaussian distribution as an approximation for the first minimum of the Bessel function.

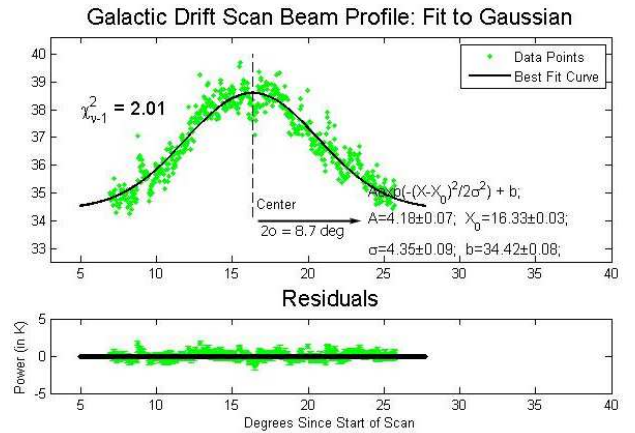


FIG. 3: Drift scan over the galactic plane around  $l = 30^\circ$ . A similar procedure is used to extract the first minimum.

and the reduction of a circularly polarized radiation to a linearly polarized receiver. We find a  $T_{sun}$  of  $3.5 \times 10^4 \text{K}$ .

$$T_{sun} = 2 \times \left( \frac{7.5^2}{.5^2} \right) \times 77.5 \text{K} = (3.5 \pm .3) \times 10^4 \text{K} \quad (3)$$

Here, we use the half-power beamwidth  $7.5^\circ$  instead of the full beamwidth in order to account for the non-uniform receiving power of the antenna. Since this result is now far above the known surface temperature of the sun ( $\sim 6000\text{K}$ ), we are led to believe that the bulk of the 21 cm radiation from the sun has its origins in its chromosphere as opposed to its surface. In another trial, we allow a portion of the galactic plane around  $l = 30^\circ$  to drift through our beam width. See Figure 3. The  $2\sigma$  width is now  $8.7^\circ$ . We use a simplified model and treat both solar and galactic emissions as

step functions to be convolved with the diffracting beam pattern. We estimate the bulk emission from this part of the galaxy to be coming from an angular region approximately  $8.7 - 5.48 - 0.5 = (2.7 \pm 0.2)^\circ$  across.

## 6. EXPLORING GALACTIC STRUCTURE AND DYNAMICS

Recalling that the sharpness of the 21-cm hydrogen line allows for very precise doppler spectroscopy, we make use of the abundance of neutral hydrogen in the Milky Way to derive a galactic rotation curve (a  $v(r)$  for every  $r$ ). We model the galaxy as a differentially rotating thin disk with stellar and interstellar material in circular orbits around a shared origin. This symmetry assumption allows the average velocity to be independent of polar angle  $\phi$ ,  $\frac{\partial \bar{v}}{\partial \phi} = 0$ . Knowledge of an explicit velocity curve then allows dramatic insight into the distribution of mass within the galaxy and eventually leads to determination of galactic structure.

### 6.1. Velocity Curve Predictions

Using Newtonian mechanics we can calculate the rotational velocity of a point mass at a distance  $r$  from a gravitational center with a total mass of  $M$ . Assuming that  $M$  is contained within a radius  $r_0$ , the orbital velocity follows the relation,

$$v(r) = \sqrt{\frac{GM}{r}} \propto \frac{1}{\sqrt{r}}, \quad r > r_0 \quad (4)$$

This is known as a Keplerian velocity curve, which is obeyed by the planets in our solar system. For the Milky Way galaxy, however, this model is unrealistic, as we well know the mass is not concentrated at the galactic center but spread out over many kpc. From observational evidence, we know the Milky Way to consist of two visible parts: a spherical central bulge with radius of approximately  $r = 1.5 \text{ kpc}$  with a constant mass density  $\rho_B$  [3], and an outer extent with luminosity falling off exponentially with  $r$ . Considering first the central bulge, integrating the constant density we find a total enclosed mass  $M(r)$  proportional to  $r^3$  and a  $v(r)$  that increases linearly in  $r$ .

Treating the outer regions is only slightly more involved. We begin with the empirically determined surface luminosity density curve for the galactic disk,  $\Sigma(r)$  in units of  $[L_\odot/\text{kpc}^2]$  [2]. Using two-dimensional geometry now, we assign an average mass-to-light ratio,  $\gamma \approx 0.6$ , to convert to surface mass density in units of  $[M_\odot/\text{kpc}^2]$ . Finally, we integrate over  $r$  to find total enclosed mass

at a given radius:

$$\begin{aligned} M(r) &= \int_0^r [\gamma \Sigma(r)](2\pi r) dr = \int_0^r [\rho_0 e^{-r/b}](2\pi r) dr \\ M(r) &= \rho_0 \left[ b^2 \left( 1 - e^{-r/b} \right) - r b e^{-r/b} \right] \end{aligned} \quad (5)$$

Here,  $b$  is a characteristic radius, taken to be about 3 kpc, and  $\rho_0$  is the maximum surface mass density. From there we can quickly derive a  $v(r)$  using the relation  $v(r) = \sqrt{GM(r)/r}$ . We find that the limiting behavior for  $v(r)$  at large  $r$  is also Keplerian (goes as  $1/\sqrt{r}$ ). Since in reality, we will be observing clumps of gravitating matter as opposed to a single point mass, the  $v(r)$  from here on will represent an average velocity.

### 6.2. Experimental Methods

We point our telescope to various galactic longitudes  $l$  and collect doppler shifted 21-cm spectra. However, there is no way to separate the accumulated received radiation by source distance. In order to derive a rotation curve, we will need to be able to associate each measured velocity with a non-ambiguous radius. We do this by considering only the maximum red/blue shift in each direction. We propose that within  $0 < l < 90$ , the maximum recessional velocity corresponds to the matter traveling directly away from us in a circle of radius  $R$  that is tangent to our line of sight, assuming a relatively flat rotation curve, due to the maximization of the dot product  $\vec{v} \cdot \vec{s}$ , where  $\vec{s}$  is the line of sight. This is best understood with a diagram (Figure 4).

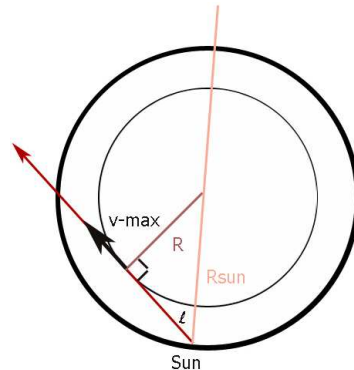


FIG. 4: The maximum recessional velocity along a line of sight corresponds to matter moving in a circle with radius  $R$  around the galactic center.

The only visible portion of the galactic plane suitable for this analysis has  $0 < l < 90$ . We sweep this range to find maximal  $v_{rec}$  in each direction and use trigonometry to find its associated radius  $R = R_\odot \sin(l)$ .

### 6.3. Calibration

We use a frequency generator to conduct a 3-point calibration of our output. This procedure converts each bin in our accumulated spectrum into a calibrated frequency value. We obtain calibration errors through a linear fit.

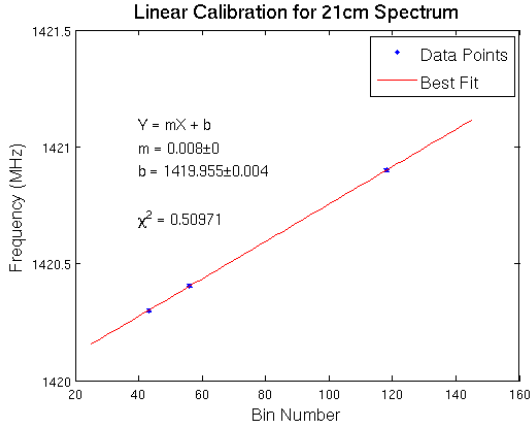


FIG. 5: Calibration of spectrum. Frequency vs. bin number.

### 6.4. Corrections - VLSR and Dispersion

Two key corrections were made to our raw data in order to obtain the velocity profile. First, in order to account for the velocity dispersion due to relative motion of gas clusters in a given region of the galaxy, we point our telescopes exactly anti-center, at  $l = 180^\circ$ . Since we expect no net red- or blueshift in this direction (average motion perpendicular to our line of sight), the width of the spectrum can be used to determine a representative velocity dispersion. See Figure 6. We subtract this expected dispersion from the maximum redshift along our line of sight to find the maximum *average* recessional velocity.

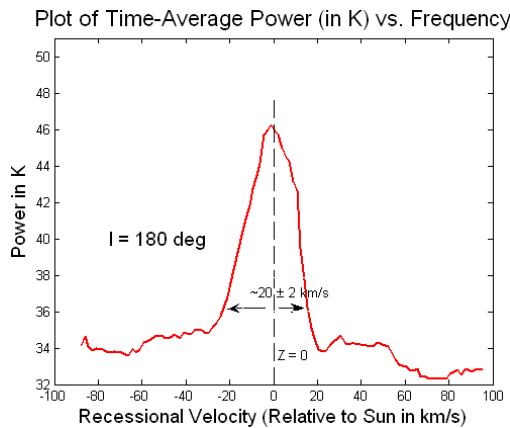


FIG. 6: 21cm power spectrum obtained from observation along  $l = 180$ . We find the velocity dispersion to be approximately 20km/s.

A second correction of importance removes the effect of the receiver's motion relative to the galactic center. This includes earth's 30 km/s orbit around the sun and the sun's 20 km/s motion in the direction of RA 18h Dec  $30^\circ$  relative to the local standard of rest (LSR). We use vector geometry to calculate the component of this combined motion along our line of sight. See Figure 7.

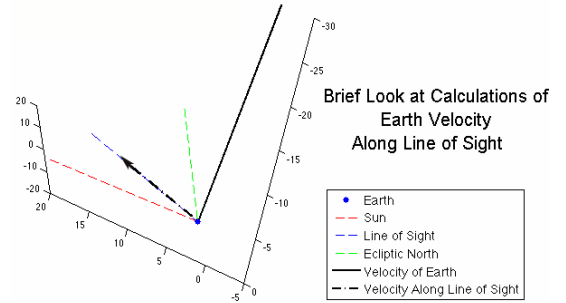


FIG. 7: VLSR correction geometry.

Finally, the rotational velocity of the source can be derived from the corrected recessional velocity and the galactic longitude using the following relation which takes into account the orbital motion of the LSR around the galactic center,

$$v = v_{rec} + v_{LSR} \sin(l) \quad (6)$$

### 6.5. Data and Results

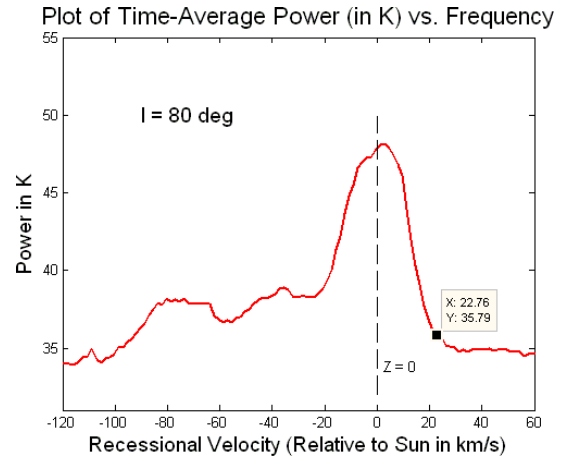


FIG. 8: Spectrum taken at galactic longitude  $80^\circ$  and latitude  $0^\circ$ . The integration time is approximately 5 minutes.

A sample spectrum is shown in Figure 8. We found the maximum redshift in this case to be about 22.8 km/s, and an average recessional velocity of approximately 3 km/s after dispersion factors have been accounted for.

A sweep from longitude 80 to longitude 5 was made with spectra taken every 5 degrees. We found there to

| $l$ | Radius | Sigma Radius | Relative Velocity | Sigma Velocity |
|-----|--------|--------------|-------------------|----------------|
| 90  | 7.97   | 0.43         | 0                 | 2.00           |
| 80  | 7.85   | 0.42         | 2.76              | 3.61           |
| 75  | 7.70   | 0.42         | 2.07              | 3.61           |
| 70  | 7.49   | 0.41         | 9.72              | 3.61           |
| 65  | 7.22   | 0.39         | 18.34             | 4.47           |
| 60  | 6.90   | 0.38         | 36.55             | 5.39           |
| 55  | 6.53   | 0.36         | 52.31             | 7.28           |
| 50  | 6.11   | 0.34         | 63.92             | 8.25           |
| 45  | 5.64   | 0.32         | 68.06             | 10.20          |
| 40  | 5.12   | 0.30         | 75.83             | 13.15          |
| 35  | 4.57   | 0.27         | 95.7              | 13.15          |
| 30  | 3.99   | 0.25         | 109.4             | 15.13          |
| 25  | 3.37   | 0.22         | 115.3             | 20.10          |
| 20  | 2.73   | 0.20         | 133.9             | 20.10          |
| 15  | 2.06   | 0.17         | 63.11             | 15.13          |
| 10  | 1.38   | 0.16         | 33.01             | 11.18          |
| 5   | 0.69   | 0.14         | 15.86             | 8.25           |

TABLE I: Table of corrected recessional velocities  $v_{rec}$  obtained for each radius  $r$ .

be a general smearing of the spectrum as we neared the galactic center due in part to the increased noise (decreased pointing elevation) and in part to the additional thickness of the emitting region and increase in velocity dispersion. The derived rotation curve using the methods outlined in section 6.2 is given in Table I and Figure 9 with comparison to Keplerian and visible matter predictions plotted with dashed lines.

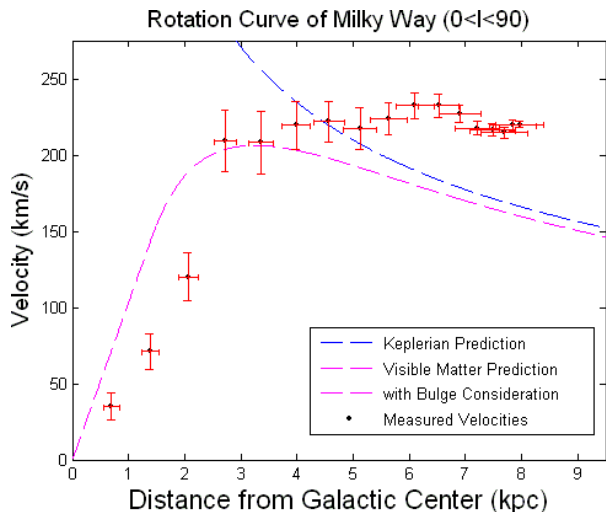


FIG. 9: Rotation curve for the Milky Way galaxy for  $R \leq R_{\odot}$ . Comparison to expected velocity functions.

## 6.6. Discussion

We see clearly non-Keplerian behavior in our rotation curve. For small  $R$ , the rotational velocity rises linearly in  $r$  as predicted by the bulge model, however for large  $R$  the observed behavior deviates significantly from the

expected Keplerian  $1/\sqrt{r}$  decay. In fact, the rotation curve appears to be a constant for  $R > 2.5 kpc$  and shows no indication of falling off.

A possible explanation for this phenomenon is a proposed dark matter halo surrounding the visible matter in the galaxy with a mass density  $\rho_d(r)$  that falls off as  $1/r^2$  [1]. Integrating  $\rho_d$  over a sphere indicates a total enclosed mass  $M(r)$  proportional to  $r$ , and a constant rotational velocity,  $v(r)$ . It is proposed that this dark matter halo extends many kpc beyond the orbital radius of the sun and the rest of the visible galaxy. Beyond this dark halo, the velocity curve is expected to be Keplerian.

## 6.7. Spiral Arms of the Milky Way

Revisiting our 21cm spectra we notice that there is more information contained within the peaks than the simple maximal recessional velocity which we used in the previous few sections to derive the rotational curve of the galaxy. In order to extract information about galactic structure, we turn to the relative intensities at different redshifts. Extrapolating between the data points on our rotation curve, we plot the locations of the maximas, assuming these to be the regions of highest H1 concentration, along our line of sight in each direction  $l$ . Trigonometry is helpful in deriving these relations.

We determine geometrically radius  $r$  and angle  $\theta$  of these maxima given the corresponding  $v_{rec}$  and  $l$ . We interpolate the given  $v_{rec}$  in the following function for  $r$ :

$$v_{rec}(r) = F(r, v(r)) = \sin(l) \left[ \frac{r_{\odot}}{r} v(r) - v_{LSR} \right] \quad (7)$$

From  $r$ , we can now find the angle  $\theta$ :

$$\theta(r) = G(r) = \pi - \left( l + \sin^{-1} \left[ \frac{r_{\odot}}{r} \sin(l) \right] \right) \quad (8)$$

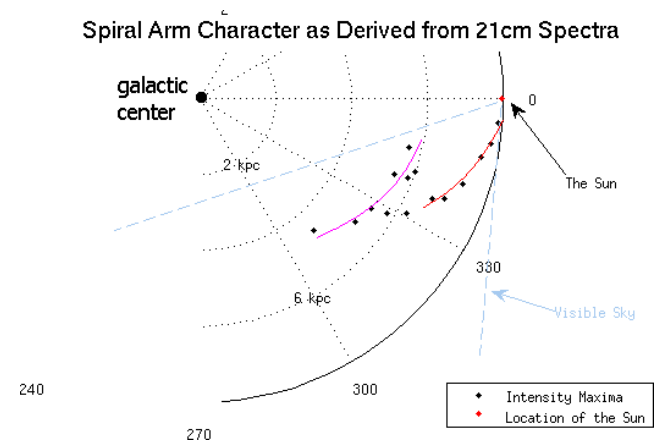


FIG. 10: Plot of the sources of maximum intensity 21 cm emission between  $30 < l < 80$ . We see possible evidence of two distinct density waves (spiral arms) of high H1 concentration.

Performing this analysis for each redshifted peak along  $30 < l < 80$ , we obtain the following polar plot showing

the locations of highest H1 density in the viewable portion of the galactic plane (Figure 10). There is evidence of some spiral structure as indicated by two possible arms of high density H1 gas, whose locations are approximated by superimposed curves to aid viewing. The outer curve is likely the Orion arm, of which the solar system is a part, and the inner may be a short portion of the Sagittarius Arm.

## 7. ERRORS

The empirically determined parameters used in this experiment, as a whole, were a surprisingly large contributor to general error. The orbital radius of the sun,  $R_{\odot}$ , for example, is only known to approximately 6-10% accuracy, and was the largest contributor to uncertainty in  $r$  in our galactic rotation curve. Similarly,  $v_{LSR}$  and  $v_{\odot}$  were known only approximately. Systematic inaccuracy of our results may have resulted from these uncertainties.

After an initial confusion regarding the dipole noise generator (the result of a poor connection), very little error can be attributed to our electronics. Calibration errors became negligible after all other factors were taken into consideration. The pointing error, determined by repeated scans of the sun, was approximately  $2^{\circ}$  and were corrected occasionally with offsets to eliminate its systematic effects.

The need for a radio-quiet environment for high-accuracy radio astrophysics became apparent after only a few trials. Aside from noise within the electronics (temperature calibrations determine  $T_{sys}$ ), radio towers, cell phones, even satellites distorted our spectra immensely. Although mostly contributing a noise floor, as we moved to lower galactic longitudes and therefore nearer to the horizon, not only were there occasionally loud signals that blotted out the entire spectrum, but the noise floor also shifted and began to take on some slope. This made determination of maximum redshift difficult and although we attempted to correct for this effect by taking a noise background at a similar elevation away from the galactic plane, contributed significantly to our error in the lower longitudes.

Non-validity ranges in some of our assumptions is a matter of greater concern. These errors contribute systematically to our results and may result in significant corrections and shifts. The assumption that  $v(r)$  is mostly flat and therefore the highest recessional velocity

corresponds to the radius of closest approach is obviously called into question by our velocity curve itself. Wrong attributions of maximal velocity would result in an overestimate of  $v(r)$  at small  $r$ . In addition, the assumption of perfectly circular rotation around the galactic center is refuted by evidence of spiral arms of high mass density with radial components. To some extent, this will affect our velocity curve, but to a greater extent, it will change the locations of the maxima in our plot of density maxima and warp our spiral arms.

We would like to also point out certain limitations to our method in estimating velocity dispersion. Since stronger gravitational interactions would likely result in a wider distribution of velocities, regions of lower stellar density would not necessarily suffer the same dispersive forces as regions of higher stellar density. This would result in an underestimate of certain velocities and an overestimate of others.

## 8. CONCLUSIONS

In the earlier portions of our lab, we determined the chromospheric temperature of the sun to be approximately  $(3.5 \pm .3) \times 10^4$  K, and the full beamwidth of the telescope to correspond to a the circular diffraction theory's prediction of  $1.22\lambda/D$ . Additionally, we measured the thickness of the peak 21cm emitting hydrogen in the region of galactic longitude  $30^{\circ}$  and found it to be approximately  $(2.7 \pm 0.2)^{\circ}$  in angular extent.

In the latter parts of our experiment we went into some detail investigating the dynamics and structure of the Milky Way galaxy. We derived a rotation curve from doppler spectroscopy performed on 21-cm H1 emissions and found it to be non-Keplerian in nature, indicating some misalignment between the expected gravitational effects due to visible matter and the actual dynamics of our galaxy. We offered the existence of a dark matter halo as a possible explanation of this phenomenon, supported by our experimental results. Additional analysis of the 21-cm spectra in various directions in the galactic plane indicated the presence of 2 possible spiral arms. Due to the large uncertainties in this particular analysis the results are interesting but inconclusive and definitely warrants further investigation. In the end, we believe we have demonstrated the 21-cm neutral hydrogen line to be a powerful tool for exploring our galaxy and beyond.

---

[1] Drees, M. "Dark Matter". Technical University, Munich. [2003]  
 [2] Mihos, Chris. "Rotation Curves". Case Western Reserve University. <http://burro.astr.cwru.edu/> [2001]  
 [3] University of Oregon Physics. <http://physics.uoregon.edu/~jimbrau/> [2001]  
 [4] "Diffraction from a Circular Aperture". Paul Padley, Con-

nexions. [2005]  
 [5] Sewell, "21 cm Radio Astrophysics", 8.14 Course Reader, [2007]  
 [6] van de Hulst, H.C., Muller, C.A., Oort, J.H. "Spiral Structure... Derived from Hydrogen Emission at 21cm Wavelength". Bulletin of Astronomical Institutes of Netherlands. Volume XII. Number 452. [1954]

- [7] Shu, F.H. "Our Galaxy: The Milky Way System". The Physical Universe - Chapter 12. University Science Books. [1982]

### **Acknowledgments**

All non-linear fits were made with the MATLAB scripts made available to us on the Junior Lab website: <http://web.mit.edu/8.13/www/jlmatlab.shtml>.

We would like to thank the Junior Lab staff for their assistance and Scott Sewell in particular for fixing the telescope repeatedly and in many ways so that this experiment can be possible.